Assessment of Accuracy of MODIS Sea Surface Temperature at High Latitudes Using Saildrone Data

Chong Jia , Peter J Minnett * , Malgorzata D Szczodrak

Posted Date: 6 May 2024

doi: 10.20944/preprints202405.0250.v1

Keywords: MODIS; sea surface skin temperature; Saildrone; validation; Arctic

Article

Assessment of Accuracy of MODIS Sea Surface Temperature at High Latitudes Using Saildrone Data

Chong Jia [1], Peter J. Minnett [2,*] and Malgorzata Szczodrak [2]

[1] Graduate Program in Meteorology and Physical Oceanography, Rosenstiel School of Marine, Atmospheric, and Earth Science, University of Miami, Miami, FL, USA; chong.jia@earth.miami.edu

[2] Department of Ocean Sciences, Rosenstiel School of Marine, Atmospheric, and Earth Science, University of Miami, Miami, FL, USA; gszczodrak@earth.miami.edu

* Correspondence: pminnett@earth.miami.edu

Abstract: The infrared (IR) satellite remote sensing of sea surface skin temperature (SST_{skin}) is challenging in the northern high latitude region, especially in the Arctic because of its extreme environmental conditions, and thus the accuracy of SST_{skin} retrievals is questionable. Several Saildrone uncrewed surface vehicles were deployed at the Pacific side of the Arctic in 2019, and two of them, SD-1036 and SD-1037, were equipped with a pair of IR pyrometers on the deck whose measurements have been shown to be useful in the derivation of SST_{skin} with sufficient accuracy for scientific applications, providing an opportunity to validate satellite SST_{skin} retrievals. This study aims to assess the accuracy of MODIS-retrieved SST_{skin} from both Aqua and Terra satellites by comparisons with collocated Saildrone-derived SST_{skin} data. The mean differences in SST_{skin} from the SD-1036 and SD-1037 measurements are different by ~0.4 K, largely resulting from differences in the atmospheric conditions experienced by the two Saildrones. The performance of MODIS on Aqua and Terra in retrieving SST_{skin} is comparable. Negative brightness temperature (BT) differences between 11 μm and 12 μm channels are identified as being physically based, but are removed from the analyses as they present anomalous conditions for which the atmospheric correction algorithm is not suited. Overall, the MODIS SST_{skin} retrievals show negative mean biases, -0.234 K for Aqua and -0.295 K for Terra. The variations in the retrieval inaccuracies show an association with diurnal warming events in the upper ocean from long periods of sunlight in the Arctic. Also contributing to inaccuracies in the retrieval is the surface emissivity effect in BT differences characterized by the Emissivity-introduced BT difference (EΔBT) index. This study demonstrates the characteristics of MODIS-retrieved SST_{skin} in the Arctic, at least at the Pacific side, and underscores that more in situ SST_{skin} data at high latitudes are needed for further error identification and algorithm development of IR SST_{skin}.

Keywords: MODIS; sea surface skin temperature; Saildrone; validation; Arctic

1. Introduction

Satellite remote sensing offers the best way of providing long-period, frequent, global sea surface temperature (SST) maps, which are vital for understanding the climate [1,2], monitoring long-term climate trends [3] and studying some weather systems, such as hurricanes [4,5] and El Niño/La Niña events [6,7], and in supporting weather and ocean forecasting. Currently, measurements from both infrared (IR) and microwave radiometers aboard satellites can be used to derive SSTs, but the IR sensors have a higher spatial resolution with a longer historical record, including the Advanced Very High-Resolution Radiometer (AVHRR) [8], Moderate Resolution Imaging Spectro-radiometer (MODIS) [9], Visible Infrared Imaging Radiometer Suite (VIIRS) [10], Sea and Land Surface Temperature Radiometer (SLSTR) [11] and Visible and Infrared Scanning Radiometer (VIRR) [12]. They use radiometric measurements at wavelengths of 3.7-4.1 μm and/or 10-12 μm interval to derive SSTs. However, both bands are sensitive to the presence of clouds, interactions with aerosols and

 doi:10.20944/preprints202405.0250.v1

absorption by atmospheric water vapor. Thus, thermal IR measurements for deriving SST require atmospheric correction of the measured signals and can only be made in cloud-free conditions. Furthermore, the retrieval of IR satellite SST at high latitudes, particularly in the Arctic region, poses several challenges [13,14], primarily due to the extreme environmental conditions in this area, such as the persistent cloud cover and long twilight [15], sea ice presence introducing complications in distinguishing open water from ice-covered regions [16] and the occurrence of extremely cold and dry atmospheres compared with other areas of the global ocean [17].

In addition to being a climatological extreme, the Arctic is a vast and remote region with limited access for in situ measurements, resulting in difficulties in the accuracy assessment of satellite-derived SST and larger uncertainties in the retrievals. As elsewhere, in situ measurements of subsurface SST taken by drifting buoys are the main source of validating data at high latitudes. Their sparsity is much more significant at the northern Pacific side of the Arctic region, incorporating Beaufort Sea, Chukchi Sea and East Siberian Sea, in contrast to the Greenland, Norwegian, and Barents Seas in the Atlantic Ocean sector, which feature extensive year-round open water at similar latitudes. However, the sea ice melt-back in recent years, especially during warmer months, has led to an improvement in the number of in situ SST data in the Arctic, which is advantageous to the accuracy assessment and refinement of the atmospheric correction algorithms for SST retrieval [17–19].

Nevertheless, different from the sea surface skin temperature (SST_{skin}) derived from the IR emission from within the conductive laminar sub-layer of ~10-20 μm thickness beneath the air-sea interface detected by IR radiometers, buoys take the ocean temperature referred to as SST_{depth} at depths of several centimeters to tens of meters [20]. The difference between SST_{skin} and SST_{depth} mainly comprise the cool skin effect and diurnal warming. The cool skin effect, which means SST_{skin} is cooler than SST_{depth}, nearly always exists, resulting from the heat loss through the oceanic skin layer to the atmosphere, supplied by the sensible and latent heat fluxes and the net longwave radiation [21]. But such difference can be overwhelmed by the thermal stratifications in the daytime caused by the strong insolation under low wind speeds, i.e., diurnal warming [22,23]. Therefore, using subsurface temperature, SST_{depth}, to validate IR satellite-derived SST_{skin} may wrongly attribute some contributions of cool skin and diurnal warming to the inaccuracies of satellite retrievals, underscoring the necessity of collecting SST_{skin} using measurements from IR radiometer systems on the ships or other platforms. Some noteworthy progress has been made with several successful instruments being deployed over the past few decades, such as the Marine Atmospheric Emitted Radiance Interferometer (M-AERI) [24], the Calibrated Infrared In situ Measurement System (CIRIMS) [25] and the Infrared Sea surface temperature Autonomous Radiometer (ISAR) [26]. However, the amount of in situ SST_{skin} data is still lacking with limited spatio-temporal extent, especially for high latitude regions, primarily due to the difficulty and the high cost of deployment on ships, and maintenance of those accurate IR radiometers.

The uncrewed surface vehicles (USVs) are more cost-effective than traditional research vessels. To fill the gap of SST_{skin} data at high latitudes, especially at the Pacific sector of the Arctic, two Saildrone USVs were deployed in the 2019 Arctic Cruise of the 3rd Multi-Sensor Improved Sea Surface Temperature Project (MISST-3) [27,28] carrying a simple system with two IR radiation pyrometers on the deck to collect the measurements for deriving SST_{skin}. Although this configuration was experimental, Jia, et al. [29] have demonstrated that the accuracy of Saildrone-derived SST_{skin} is sufficient for use in scientific research after controlling for quality. Few papers used the Saildrone data to validate either Level-2 satellite SST products or Level-4 SST analyses [30,31], but only SST_{depth} measurements at -0.6 m from CTD sensors were used for comparisons. Hence, this paper will utilize the unique Saildrone SST_{skin} dataset at high latitudes to assess the accuracy of MODIS-retrieved SST on the NASA Earth Observing System (EOS) satellites Terra and Aqua, improving the understanding of error characteristics of MODIS SST in the northern Pacific side of the Arctic.

The paper will be organized as follows. The MODIS-retrieved SST_{skin}, Saildrone-derived SST_{skin}, and other ancillary data are introduced in Section 2. The statistical results of the MODIS-Saildrone

 doi:10.20944/preprints202405.0250.v1

comparisons are presented in Section 3. The results of the error analysis are discussed in Section 4 associated with several influential factors. The conclusions are made in Section 5.

2. Data and Methods

2.1. MODIS SST Data

The goal of MODIS SST_{skin} processing at NASA is to develop and apply consistent atmospheric correction and cloud detection algorithms to long-wave IR (LWIR) measurements to derive SST_{skin}; the algorithms were developed at the University of Miami's Rosenstiel School of Marine, Atmospheric, and Earth Science [9,17,32,33]. The NASA Ocean Biology Processing Group (OBPG) applies the algorithms to generate Level-2 SST_{skin} using the Multi-Sensor Level-1 to Level-2 software (l2gen). The current MODIS LWIR SST_{skin} retrieval algorithm is a modified version of the nonlinear SST formulation of Walton, et al. [34] as given below:

$$SST_{sat} = a_0 + a_1 BT_{11} + a_2 (BT_{11} - BT_{12}) T_{sfc} + a_3 (\sec\theta - 1)(BT_{11} - BT_{12}) + a_4 (mirror) + a_5 (\theta) + a_6 (\theta^2) \quad (1)$$

where SST_{sat} is the satellite-derived SST_{skin}, BT_{11} and BT_{12} are brightness temperatures (BTs) in the 11 μm and 12 μm wavelength bands; T_{sfc} is a reference SST; *mirror* represents the mirror side number with a value 0 or 1; θ is the sensor zenith angle. Coefficients a_0-a_6 are derived by regression of matchups between the in situ and satellite measurements for each month of the year with latitude-band dependence. The algorithm is described in detail by Kilpatrick, et al. [9] and Jia and Minnett [17].

The standard Level-2 MODIS SST_{skin} fields can be accessed through the ocean color web or Physical Oceanography Distributed Active Archive Center (PO.DAAC). Each SST_{skin} retrieval contains a numeric Quality Level (QL) assigned by running a series of tests, with QL = 0 being the best quality and QL = 4 being the worst. Note that data with QL > 1 are not recommended to be used for scientific studies as they may have significant cloud contamination identified by the cloud classifier algorithm presented in Kilpatrick, et al. [32] or other problems related to sea ice or dust.

2.2. Saildrone Cruises and Data

2.2.1. Saildrone Arctic Cruises

Saildrone is an advanced, wind-driven, USV manufactured by Saildrone Inc. located in Alameda, CA. It carries a number of solar-powered scientific instruments to collect high-frequency (1-min sampling interval) data including both oceanographic and meteorological parameters. A more detailed introduction to Saildrones is given by Jia, et al. [29]. During a collaborative NOAA-NASA mission in 2019, a fleet of six Saildrones were deployed from Dutch Harbor, Alaska in May. Five of those vehicles navigated through the Bering Strait into the Chukchi Sea, reaching up to ~75°N before making return voyages. This paper reports the assessment of accuracy of MODIS SST_{skin} using measurements from two Saildrones, SD-1036 and SD-1037, the deployments of which were funded by NASA through the National Oceanographic Partnership Program (NOPP). The navigation tracks and the configuration of two Saildrones are shown in Figure 1.

2.2.2. Saildrone Data

Other than one previous deployment, SD-1036 and SD-1037 are the only two Saildrones equipped with a "unicorn"-structure IR broadband pyrometers (8-14 μm) to facilitate the SST_{skin} derivation. Two pyrometers, manufactured by Heitronics, were installed on the deck at a height of 0.8 m above sea level, viewing the sea surface and the sky at the same nadir angle and zenith angle of 50° when the Saildrone is upright. The measurements from the sky-viewing CT09.10 sensor are used to correct for the component of the upwards radiance due to reflected downwelling atmospheric radiance at the ocean surface in the IR radiation measured by the sea-viewing CT15.10 sensor. Jia, et

 doi:10.20944/preprints202405.0250.v1

al. [29] provided the details of SST_{skin} retrieval algorithm with the error and uncertainty budget analyses, demonstrating the uncertainty of Saildrone-derived SST_{skin} is ~0.12 K without significant systematic bias after quality control. They indicate the data are suitable for the accuracy assessment of satellite SST_{skin} retrievals.

SST_{depth} was taken by several instruments onboard SD-1036 and SD-1037, for each vehicle including two CTDs, one SBE 37 and one RBR, both at a depth of -0.54 m, and seven additional SBE 56 self-recording thermometers at a range of depths from -0.33 to -1.71 m along the keel. Both CTDs and temperature loggers make measurements of SST with an accuracy of ±0.002 K, as stated in the manufacturers' specifications.

The Saildrones also provide measurements of meteorological variables simultaneously with the SST measurements (1-min interval), such as three-dimensional wind vector, surface air temperature and relative humidity, barometric pressure, Photosynthetically Active Radiation (PAR) at the surface, etc.

2.3. MERRA-2 Data

Modern-Era Retrospective analysis for Research and Applications, Version 2 (MERRA-2) [35], a global atmospheric reanalysis produced by the NASA Global Modeling and Assimilation Office (GMAO) provides useful input data for radiative transfer simulations, including atmospheric profiles of temperature and specific humidity and single-level meteorological fields. The MERRA-2 data has a spatial resolution of 0.5°(latitude) x 0.625° (longitude), and 1-hourly temporal-resolution for the surface data; 3-hourly for the vertical profile fields.

2.4. Quality Control and Collocation

As mentioned above, the Saildrone SST_{skin} data must be subjected to rigorous quality control before they can be used in this study. Initially, the measurements collected during the periods when the Saildrone was near sea ice must be pinpointed using images captured by onboard cameras and excluded from subsequent analyses, since the small-scale temperature variations caused by the melting sea ice will not be appropriately sampled in the MODIS field of view. Furthermore, the tilt angles of vehicle, resulting from both pitching and rolling, should be constrained to ±1.5° and ±5° respectively to prevent significant inaccuracies in SST_{skin} [29,36].

To generate the coefficients in the atmospheric correction algorithm and to assess the accuracy of MODIS SST_{skin} retrievals, a matchups data base (MUDB) has been established including collocated satellite and in situ observations, mostly from buoys [37]. To be incorporated into the MUDB, the MODIS-Saildrone matchups follow the same spatio-temporal criteria, i.e., the time window is within 30 min and the distance is within 10 km. However, due to the high observing frequency (1 min) of Saildrone, there can be multiple Saildrone measurements (up to 60) matched with the same MODIS pixel. For the independence of validation, only one of those is selected as a unique matchup in two reasonable ways based on either the closest timestamp or the smallest separation. As shown in Figure 2, the Aqua MODIS-Saildrone SST_{skin} differences are sensitive to the spatial discrepancy but with insignificant dependency on the time window for matchups determined by either time closest or distance smallest; similar for Terra MODIS, not shown. Such patterns were also found in Jia and Minnett [17] using the MODIS and in situ SST matchups at northern high latitudes, and were explained as the matched satellite-derived SST_{skin} away from center pixel may have a higher likelihood of cloud contaminated retrieval if the center pixel is cloudy. Therefore, the distance-smallest one-to-one MODIS-Saildrone matchups are selected for the following analyses to minimize the separation dependence.

 doi:10.20944/preprints202405.0250.v1

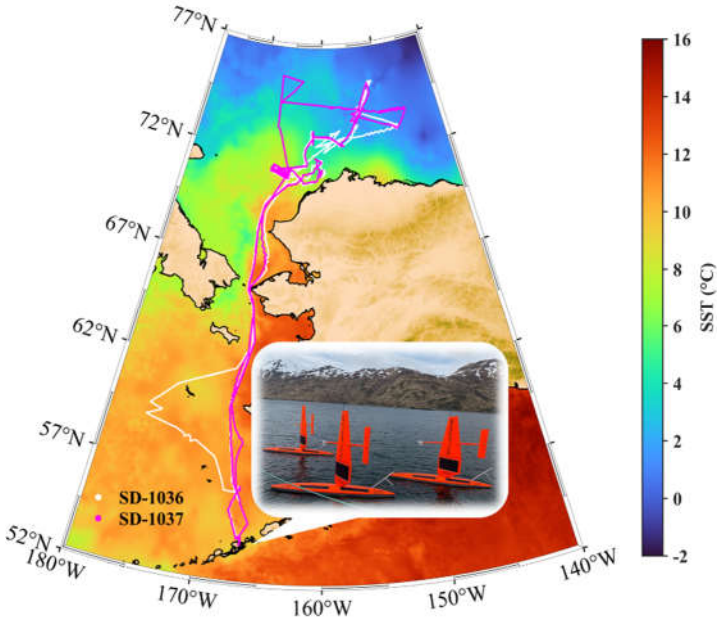

Figure 1. The cruise trajectories of two NASA-funded Saildrone vehicles, SD-1036 (white) and SD-1037 (magenta), deployed during the 2019 Arctic Cruise from 15 May to 11 October. The background SST map is taken from the Multiscale Ultrahigh Resolution (MUR) Level-4 SST analysis data [38] on September 16, 2019. The subplot is a picture of the Saildrones at the starting point is courtesy Saildrone Inc.

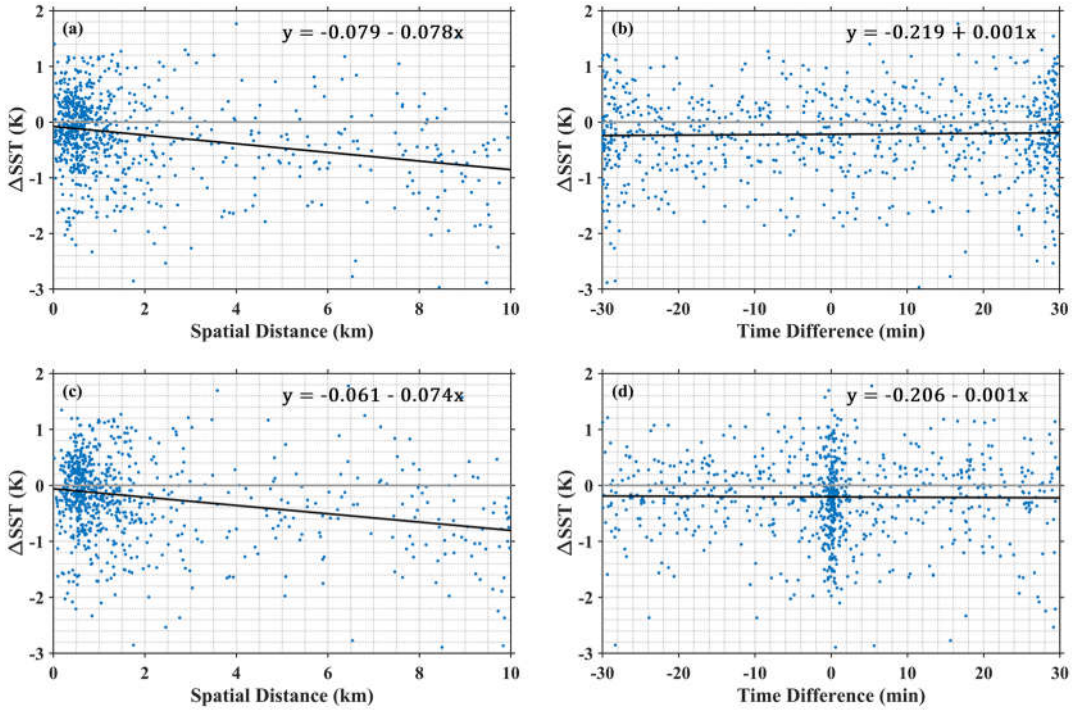

Figure 2. Aqua MODIS-Saildrone SST_{skin} difference as a function of the (a) distance and (b) time difference in the allowed spatial-temporal intervals in the matchup criteria. Data include both SD-1036 and SD-1037 measurements. The one-to-one matchups were determined based on the smallest separation between the Saildrone measurement and MODIS pixel. The black linear fitted lines are given with the expression on the top right corner. (c) and (d) are similar to (a) and (b), but for the one-to-one matchups determined by the closest timestamp.

 doi:10.20944/preprints202405.0250.v1

3. Results

Table 1 presents the statistics of the Aqua and Terra MODIS-Saildrone SST_{skin} differences during the SD-1036 and SD-1037 cruises. As expected, the performance of MODIS sensors on Aqua and Terra satellites shows comparable results. The mean biases are -0.263 K for Aqua and -0.291 K for Terra, with the overall standard deviations (STDs) of 0.741 K and 0.734 K respectively. The robust standard deviation (RSD; calculated as the interquartile range divided by 1.35) is less sensitive to the outliers and is also reported here. The RSD is 0.669 K for Aqua, while it is slightly smaller for Terra (0.559 K) indicating a fewer more extreme outliers as shown in Figure 3. Table 2 shows the statistics of matchups in terms of QL for the MODIS SST_{skin} products. The negative biases and variation are more pronounced in QL1 retrievals due to their longer atmospheric path lengths. Even though there are few scattered data points in Figure 3, the MODIS- and Saildrone-derived SST_{skin} demonstrate good quantitative agreement generally. The distributions of SST biases plotted as histograms in Figure 3 show a higher kurtosis than the Gaussian distribution; most values are concentrated into the range of -2 K to 1 K. However, there are still two things that merit attention. One is the mean and median of SST difference are significantly different using SD-1036 and SD-1037 as sources of validation data. The other one is the SST difference has an average negative bias. This section will try to address the first question, and the second one will be discussed in the next section.

Table 1. Statistics of MODIS-Saildrone SST_{skin} difference (in K), including the mean, median, standard deviation (STD), robust standard deviation (RSD), root mean square (RMS), Pearson correlation coefficient (R) and the number of valid matchup data points (Num). The statistics are shown in terms of two Saildrones and two satellites separately, including both quality level (QL) 0 and 1 data.

	Aqua			Terra		
	SD-1036	SD-1037	Total	SD-1036	SD-1037	Total
Mean	-0.073	-0.468	-0.263	-0.076	-0.490	-0.291
Median	-0.036	-0.352	-0.214	-0.021	-0.379	-0.207
STD	0.727	0.701	0.741	0.649	0.752	0.734
RSD	0.656	0.588	0.669	0.551	0.565	0.559
RMS	0.730	0.842	0.786	0.653	0.897	0.789
R	0.943	0.947	0.948	0.956	0.945	0.947
Num	411	380	791	409	444	853

Table 2. As Table 1, but statistics for different QL (also shown for each Saildrone separated by semicolon as SD1036; SD1037) of MODIS SST_{skin} retrievals.

	Aqua		Terra	
	QL = 0	QL = 1	QL = 0	QL = 1
Mean	-0.173 (-0.004; -0.345)	-0.505 (-0.239; -0.844)	-0.198 (0.034; -0.412)	-0.559 (-0.394; -0.706)
Median	-0.138 (0.057; -0.250)	-0.496 (0.315; -0.696)	-0.132 (0.064; -0.279)	-0.492 (-0.272; -0.667)
STD	0.674 (0.672; 0.631)	0.855 (0.826; 0.770)	0.690 (0.636; 0.670)	0.788 (0.581; 0.913)
RSD	0.561 (0.562; 0.529)	0.762 (0.804; 0.682)	0.500 (0.538; 0.476)	0.670 (0.639; 0.610)
RMS	0.695 (0.671; 0.718)	0.991 (0.857; 1.140)	0.717 (0.636; 0.786)	0.965 (0.700; 1.152)
R	0.956 (0.955; 0.960)	0.908 (0.914; 0.923)	0.954 (0.959; 0.956)	0.933 (0.960; 0.919)

 doi:10.20944/preprints202405.0250.v1

Num	577 (291; 286)	214 (120; 94)	631 (304; 327)	222 (105; 117)

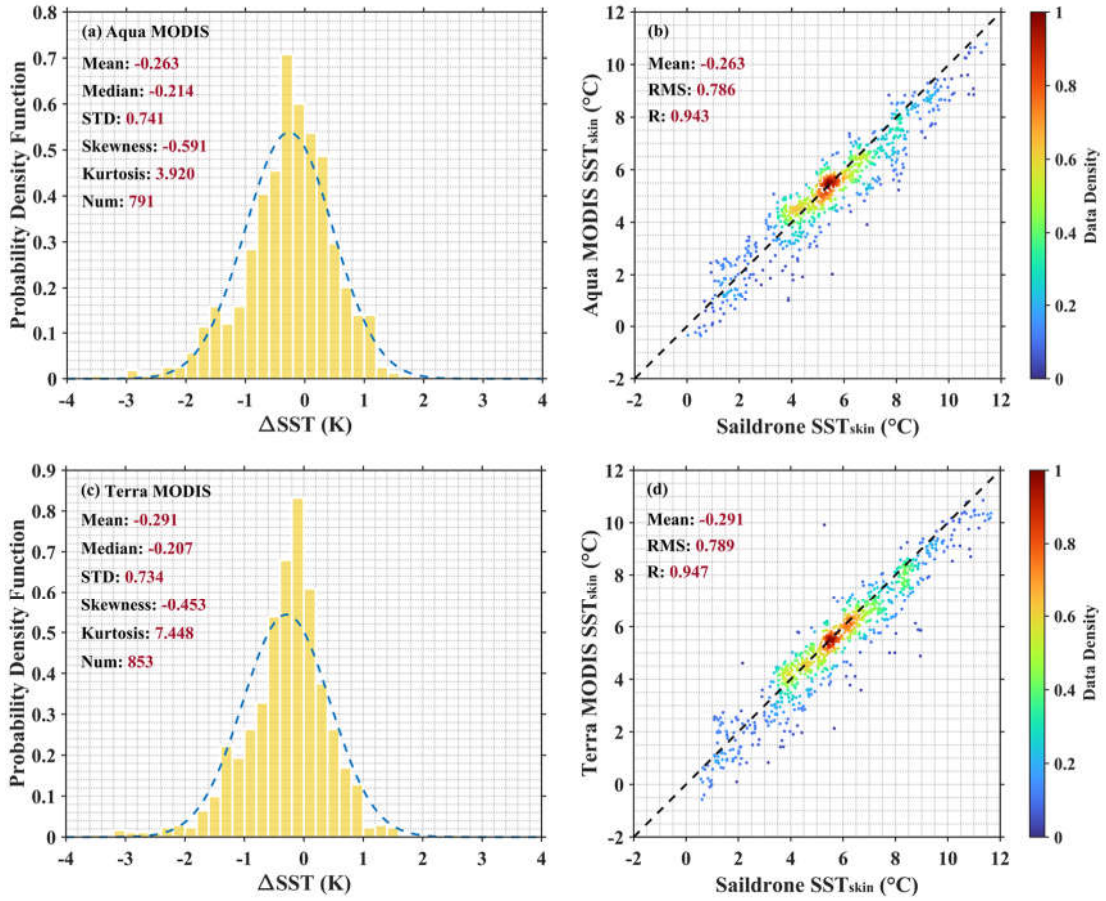

Figure 3. (a) Histogram (normal distribution fitted curve in blue) of the Aqua MODIS-Saildrone SST_{skin} difference and (b) the scatter plot of Saildrone- and MODIS-derived SST_{skin} colored by the data density. (c) and (d) are similar to (a) and (b), but for Terra MODIS-Saildrone matchups.

As presented in Jia, et al. [29], the Saildrone-derived SST_{skin} values do not possess significant systematic biases, based on some post-cruise sensor calibrations in the laboratory and congruent wind speed dependence of the cool skin effect with some previous studies [39–41]. Table 3 shows the statistics of SST comparison at various depths between SD-1036 and SD-1037 when the two Saildrones were within 1 km separation at the same time. The SST_{depth} measurements are also filtered by the platform pitch and roll angles as the SST_{skin} to minimize the tilting effect on the depth of temperature measurement. Note the discrepancies in the number of paired data at different depths are due to the missing values. The mean difference and variation of SST_{skin} are small, 0.041 K and 0.134 K, even though a little greater than those of SST_{depth}, which can be explained by three distinct factors. Firstly, the geophysical variability of ocean temperatures in the thermal skin boundary layer is likely to be larger than the subsurface temperatures resulting from the rapid response to the change of net air-sea heat flux and some surface wave processes [42]. Secondly, the inherent measurement uncertainty of radiometric instruments for SST_{skin} retrieval is much higher than that of the temperature sensors measuring at depths. Last but not least, the sampling issues may cause some biases and larger variations as the number of Saildrone SST_{skin} data is substantially smaller due to missing values. This is indicated in the SST_{depth} taken at -0.47m as well in Table 3. Nevertheless, such a difference for SD-1036 and SD-1037 SST_{skin} measurements collected within 1 km demonstrates no significant systematic biases between the two vehicles, and obviously cannot account for the big disparity (up to 0.4 K) in the mean biases of MODIS SST_{skin} when compared to the data from SD-1036 and SD-1037 separately.

 doi:10.20944/preprints202405.0250.v1

Table 3. Statistics of SST difference between SD-1036 and SD-1037 within 1 km separation measured at one time at various depths. Note that the temperature logger at -1.04 m on SD-1036 did not function.

Depth	Mean	Median	STD	RSD	RMS	R	N
0 m (skin)	0.041	0.040	0.134	0.125	0.140	0.951	237
-0.33 m	0.008	0.008	0.113	0.051	0.113	0.993	903
-0.47 m	0.023	0.010	0.095	0.080	0.097	0.993	299
-0.54 m	0.003	0.011	0.095	0.043	0.095	0.995	889
-0.81 m	-0.001	0.007	0.094	0.041	0.094	0.996	903
-1.20 m	-0.014	0.003	0.093	0.034	0.094	0.995	742
-1.42 m	-0.013	0.003	0.094	0.034	0.095	0.995	742
-1.71 m	-0.011	0.003	0.096	0.031	0.097	0.995	742

Taking the Aqua MODIS-Saildrone matchups for example, Figure 4a,b show the histogram distributions of the MODIS BT difference between 11 μm and 12 μm channels and the air-sea temperature difference (ASTD) derived from the Saildrone measurements, using SST_{skin} and surface air temperature. For the matchup dataset from the SD-1037 cruise, a larger fraction of BT differences are > 0.5 K, but with much fewer ASTDs < 0 K compared to those for the SD-1036 cruise. Figure 4c demonstrates a distinct negative relationship between the BT difference and ASTD, consistent with the distribution patterns in Figure 4a,b. Figure 5 presents the maps of ASTD and bivariate histogram for the longitude and latitude of the Aqua MODIS pixels matched with Saildrone measurements, which can further explain the more positive ASTD cases for SD-1036 matchups. Apparently, there are much more matchups during SD-1036 cruise concentrated within the range of 70-71.5°N, 160-165° W, where it has been shown that the near-surface air is likely to have been heated by its preceding passage over land [43] based on the Hybrid Single-Particle Lagrangian Integrated Trajectory (HYSPLIT; [44]) model developed by NOAA's Air Resources Laboratory, resulting in warmer air over the ocean surface. Thus, the spatial distribution difference leads to the ASTD distribution difference in the two matchup datasets that might also affect the BT difference distribution.

Theoretically, the BT difference is determined by both the sea surface boundary conditions and intervening atmosphere between surface and the satellite sensor apertures. Relevant atmospheric data from MERRA-2 have been integrated into the MODIS-Saildrone matchups based on the optimal solution for the spatio-temporal difference. Figure 6a,b are the MERRA-2 vertical profiles of specific humidity and air temperature in the lower troposphere beneath the 500 hPa level. Both of them display some differences between the matchups during SD-1036 and SD-1037 cruises. For SD-1037, the near-surface (below 940 hPa pressure level) water vapor content is significantly lower on average, and the mean air temperature is also lower at each level with a larger variability. One possible interpretation is that a few measurements in September and October are in the matchup data for SD-1037 since the IR pyrometers carried on SD-1036 were shut down because of solar power constraints starting early August while those on SD-1037 still operated until the end of mission. Similarly, there are differences in the total column water vapor distribution (Figure 6c) as well. Using MERRA-2 vertical profiles along with the surface meteorological fields taken by Saildrone as input to the RTTOV (Radiative Transfer for TIROS Operational Vertical Sounder) v13.1 model [45], results in simulated MODIS BT differences between 11 μm and 12 μm given in Figure 7. Despite possible inaccuracies in the model simulations, the general pattern shows a similarity to the observations in Figure 4a, with more frequent large BT differences in the SD-1037 matchups, confirming the dissimilar vertical atmospheric conditions contribute to diverse BT difference distributions.

All the results presented above manifest both surface and vertical atmospheric conditions are not homogeneous between the MODIS-Saildrone matched data for the SD-1036 and SD-1037 cruises, resulting in the divergence of BT difference distribution and then the statistics of the MODIS-Saildrone SST_{skin} comparisons. These differences permit the examination of the performance of the MODIS atmospheric correction algorithm in different environmental conditions. Note that the

 doi:10.20944/preprints202405.0250.v1

coefficients of SST_{skin} retrieval algorithm for MODIS in Equation (1) are derived from datasets with much bigger populations involving more variability of atmospheric conditions.

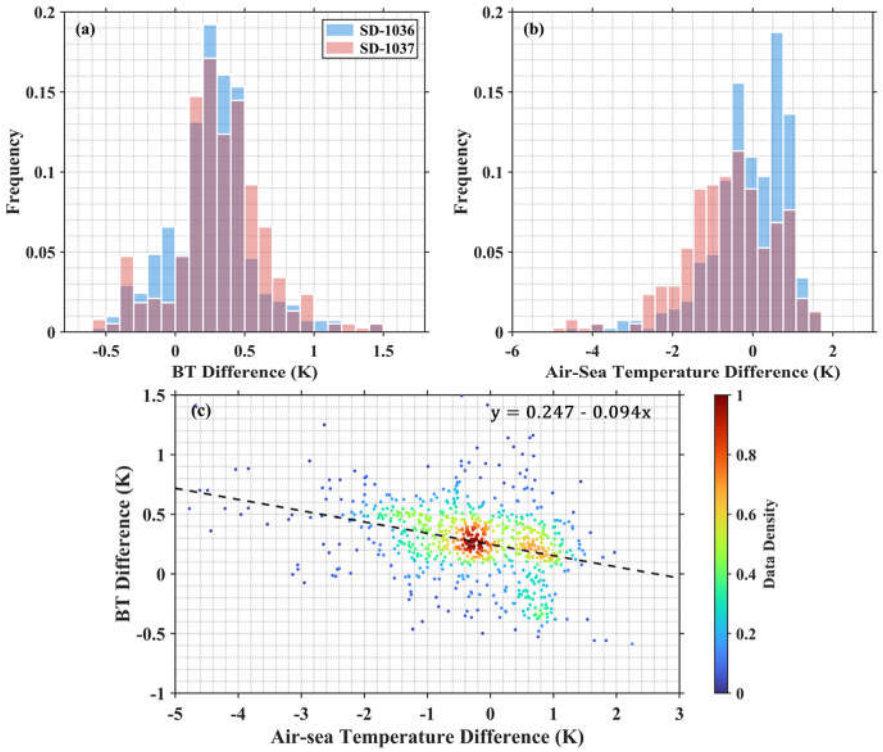

Figure 4. Histograms of (a) Aqua MODIS BT difference between 11 μm and 12 μm channels and (b) air-sea temperature difference (ASTD) for the matchup data during the SD-1036 (light blue) and SD-1037 (light red) cruises. (c) Data density scatter plot of the BT difference and ASTD in Aqua MODIS-Saildrone matchups with the fitted dashed line.

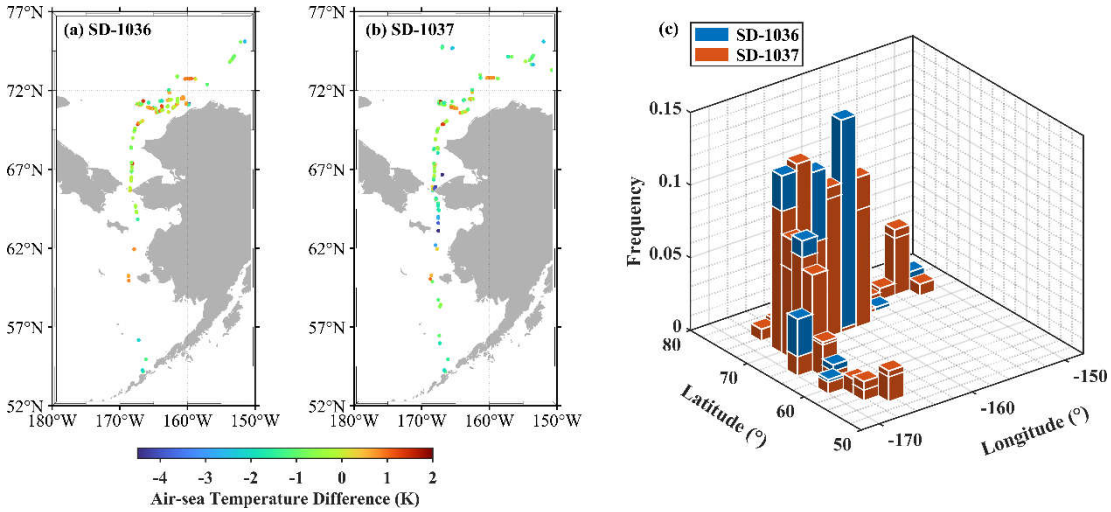

Figure 5. Maps of ASTD for Aqua MODIS-Saildrone matchups for (a) SD-1036 and (b) SD-1037. (c) Bivariate histogram for the longitude and latitude of the Aqua MODIS pixels matched with the SD-1036 (blue) and SD-1037 (red) measurements. The marks on some red columns indicate the heights of corresponding blue bars overwhelmed by the red ones.

 doi:10.20944/preprints202405.0250.v1

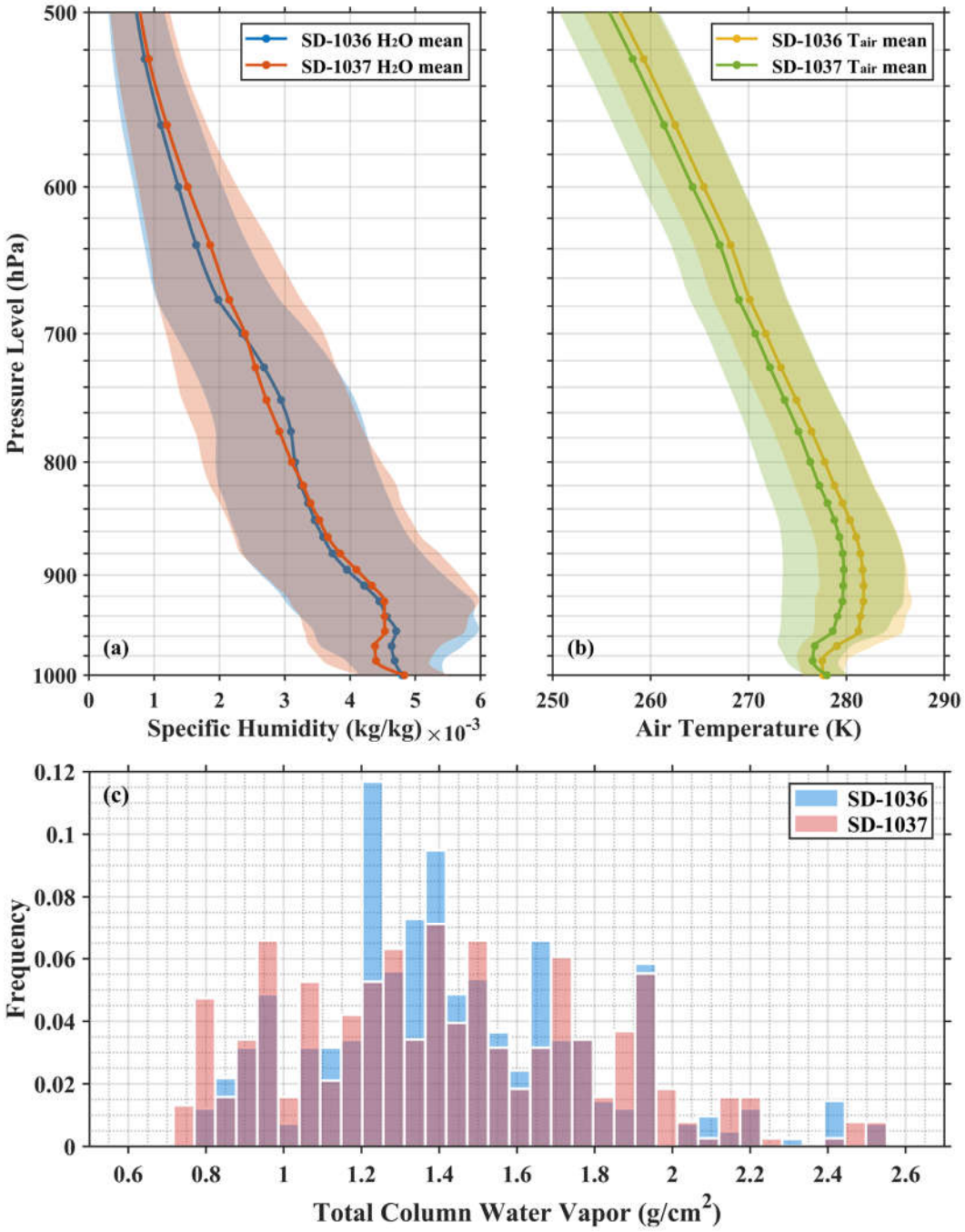

Figure 6. Reanalysis data from MERRA-2 matched with the Aqua MODIS-Saildrone matchups during the SD-1036 and SD-1037 cruises showing the vertical profiles of (a) specific humidity and (b) air temperature plotted as mean (line and dots) ±1 standard deviation (envelope), as well as (c) histogram of the total column water vapor.

 doi:10.20944/preprints202405.0250.v1

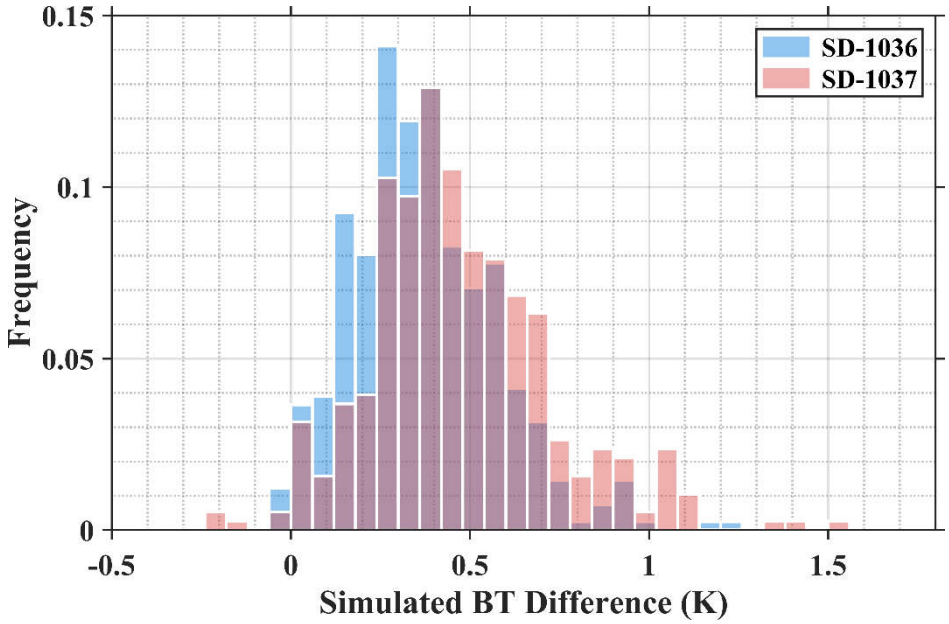

Figure 7. Histogram of RTTOV-simulated BT difference between 11μm and 12 μm for Aqua MODIS pixels matched with the Saildrone measurements during the SD-1036 and SD-1037 cruises.

To summarize, the stark differences in the mean and median values of the comparisons between the MODIS and Saildrone SST_{skin} are:

• Not caused by instrumental artifacts in the Terra and/or Aqua MODIS measurements as the comparisons are very similar for both.

• For the same reasons, they are not caused by different overpass times of the two satellites.

• For the same reasons, they are not caused by inadvertent errors in the coding or applications of cloud screening and atmospheric correction algorithms, nor in the MUDB generation for the two satellite instruments.

• Not caused by differences in the SST_{skin} retrievals from the two Saildrones, as when they were operating close together, the differences in the SST_{skin} values were small and within expectations.

The remaining likely cause of the discrepancies is in the response of the atmospheric correction algorithm to relatively small differences in the atmospheric conditions when the two Saildrones were not operating near each other; namely the different distributions of the ASTD and the lower tropospheric inversions.

4. Discussion

The major contribution to inaccuracies in the MODIS-Saildrone SST_{skin} comparisons stems from the atmospheric conditions not being fully congruent with those samples used to derive the high-latitude coefficients for the MODIS atmospheric correction algorithm [17]. As shown in Figure 4a, the majority of BT differences are positive, which is the standard situation as water vapor renders the atmosphere more emissive at 12 μm wavelengths than at 11 μm, and the normal negative atmospheric temperature lapse rate causes the signal at 12 μm wavelengths to be lower than at 11μm. This is the basis of the multi-channel algorithm that corrects atmospheric water vapor effects to derive the surface temperature. But here there are some negative values of BT differences, which can occur when temperature inversions exist in the lower troposphere, i.e., where the air temperature increases with height (Figure 6b), resulting in stronger atmospheric emission at 12 μm at these levels. The effects of negative BT differences are worthy of further study with a larger dataset or by using radiative transfer simulations. The negative BT differences in the MODIS-Saildrone matchups are discarded from part of our analyses since the current algorithm for computing SST_{skin} in Equation (1) cannot make appropriate atmospheric corrections for those anomalous conditions. Another issue is the current MODIS R2019 SST_{skin} products have a new latitude band above 60°N to derive coefficients to better represent Arctic atmospheres [17], but here there are a few matched data points located

 doi:10.20944/preprints202405.0250.v1

below 60°N (Figure 5). To be consistent with the latitudinal boundary of the algorithm coefficient generation, only measurements above 60°N are used for the following analyses. The updated statistics for the MODIS-Saildrone SST_{skin} difference after applying filters mentioned above are presented in Table 4. The mean and median MODIS SST_{skin} biases are changed slightly, but the STDs and RSDs are reduced indicating the MODIS SST_{skin} data retrieved from negative BT differences likely have larger biases. A two-sample t-test does not reject the null hypothesis and thus the SST_{skin} mean biases for MODIS on Aqua and Terra are statistically equivalent. The following analysis will take Aqua MODIS-Saildrone matchups as the example (similar for Terra MODIS, not shown) and combine the datasets for two Saildrones to identify some representative error characteristics.

Table 4. As Table 1, but after removing the MODIS-Saildrone matchups with negative BT differences and those measured below 60°N.

	Aqua			Terra		
	SD-1036	SD-1037	Total	SD-1036	SD-1037	Total
Mean	-0.057	-0.417	-0.234	-0.072	-0.501	-0.295
Median	-0.007	-0.335	-0.193	-0.022	-0.392	-0.219
STD	0.670	0.635	0.677	0.647	0.739	0.728
RSD	0.590	0.570	0.638	0.496	0.534	0.532
RMS	0.671	0.759	0.716	0.650	0.892	0.785
R	0.953	0.957	0.953	0.958	0.947	0.949
Num	325	316	641	342	370	712

Of course, the statistics of the MODIS-Saildrone SST_{skin} differences are not simply an assessment of the accuracy of the MODIS retrievals as there are some inaccuracies in the Saildrone SST_{skin} data despite of rigorous quality control, and it is conceivable that different contributions from the IR radiometers on the two Saildrone radiometer systems could cause the observed discrepancies in the statistics when compared with each Saildrone. However, Table 5 shows that there are also distinct discrepancies with comparisons between the MODIS SST_{skin} retrievals and Saildrone subsurface temperatures, which are independent of the inaccuracies in the Saildrone SST_{skin} data from each USV. This brings attention back to the inability of the atmospheric correction algorithm to compensate adequately for the surface and atmospheric effects on the measured BTs.

Table 5. Statistics of Aqua MODIS SST_{skin} difference compared with the subsurface SST_{depth} measured by temperature loggers at -0.33 m depth on the two Saildrones.

	Mean	Median	STD	RSD	RMS	R	Num
SD-1036	0.296	0.390	0.656	0.564	0.718	0.953	325
SD-1037	0.017	0.146	0.679	0.635	0.678	0.949	316
Total	0.158	0.255	0.681	0.605	0.699	0.949	641

Due to the midnight sun during the Arctic summer, only very few (< 5%) nighttime data are in the valid matchups. As introduced in Section 1, the SST_{skin} can be expressed as the combination of SST_{depth}, cool skin effect and diurnal warming, if present, in the upper ocean:

$$SST_{skin} = SST_{depth}(z) + \Delta T_c + \Delta T_{dw}(z) \quad (2)$$

where ΔT_c represents the cool skin effect and ΔT_{dw} is the diurnal warming at the depth z. ΔT_c can be parameterized with a single dependence of the wind speed as presented in some previous studies [39–41,46,47] with the same form of exponential equation but different coefficients derived using different datasets under various environmental conditions in the global ocean. Jia, et al. [43] used the nighttime data from both SD-1036 and SD-1037 to provide new parameterizations for the cool skin effect in the Pacific sector of the Arctic Ocean:

 doi:10.20944/preprints202405.0250.v1

$$\Delta T_c = -0.41 * \exp(-U_{10}/2.5) - 0.15 \quad (3)$$

where U_10 is the 10 m wind speed converted from Saildrone anemometer measurements using a logarithmic wind profile. Equation (3) then could be reasonably used to estimate the cool skin effect for the MODIS matched data along the Saildrone deployment tracks in this study. Further, the magnitudes of diurnal warming in the top 1.7 m of the ocean can also be estimated based on Equations (2) and (3). As shown in Figure 8a, large diurnal warming events (> 3 K) were identified in the matchups, and have been analyzed in detail by Jia, et al. [43]. The MODIS-Saildrone SST_{skin} differences tend to be more negative with greater amplitude of warming, indicating the underestimation of MODIS SST_{skin} retrievals under strong diurnal warming conditions. This can be interpreted as the non-representative algorithm coefficients in Equation (1) for those cases since the coefficients are derived based on a high-quality subset in the MUDB under wind speeds > 6 m/s with other constraints, whereas the strong diurnal warming occurs at low winds. Similarly, both Merchant, et al. [48] and Zhang, et al. [49] demonstrate the IR satellite SST_{skin} retrievals noticeably underestimate the diurnal variability, in the tropical Atlantic and Pacific Oceans. Note that the warming events > 0.5 K in the matchups during the SD-1037 cruise are ~10% more than those for the SD-1036 deployment, and such distribution differences might also contribute to the MODIS SST_{skin} mean biases discrepancy validated by the data from two USVs.

Another insight is that it is inappropriate to use subsurface SST_{depth} measurements to validate the satellite data mostly collected in the daytime at high latitudes in summer. Using SST-0.33 m taken from Saildrones to compare with the MODIS SST_{skin}, Table 5 shows the statistics of mean and median become positive due to the existence of diurnal warming, and those would apparently mislead the error characteristics analysis for MODIS SST_{skin} in terms of the performance of the atmospheric correction algorithm.

Since the algorithm coefficients in Equation (1) are derived using buoy measured SST_{depth}, the first term, a constant a_0, is reduced by 0.17 K to compensate for the cool skin effect. However, based on Equation (3), the mean cool skin effect for MODIS SST_{skin} retrievals along the tracks of SD-1036 and SD-1037 are estimated as -0.242 K and -0.238 K respectively, indicating the use of -0.17 K which is considered as the global average cool skin effect is inappropriate, at least for the northern high latitude regions. Such biases are not explicit in the statistics mainly because of being overwhelmed by diurnal warming. The more negative cool skins imply the generally stronger surface net heat loss from the thermal skin layer into the atmosphere. A physical skin effect scheme would be preferable instead of the -0.17 K correction for the retrieval algorithm, including the models of cool skin, but also the possible warm skin effect [36].

Jia and Minnett [17] revealed the reality of a weak correlation between the MODIS BT difference, BT_{11}-BT_{12}, and the total column water vapor at latitudes above 60°N, and proved that the sea surface emissivity effect could be dominant in the measured BT difference, amplified by the temperature difference between the sea surface and the atmospheric column throughout surface to the satellite sensor. To correct this emissivity effect, Jia and Minnett [17] introduce an index, Emissivity-introduced BT Difference (EΔBT), with the functional form as:

$$E\Delta BT = (\varepsilon_{11} - \varepsilon_{12}) * (T_s - \overline{T_a}) \quad (4)$$

where ε_{11} and ε_{12} are the sea surface emissivities at 11 μm and 12 μm wavelengths. T_s is the surface temperature and $\overline{T_a}$ is the effective air temperature at 11 μm and 12 μm associated with the atmospheric downward radiance reaching the surface.

By running the RTTOV model with the same inputs described in Section 3, both surface emissivity and the downwelling emitted radiation (then converted to $\overline{T_a}$ by a modified Planck's function [17]) can be determined. As shown in Figure 8b, the MODIS SST_{skin} biases appear to be more negative for increasing EΔBT values when EΔBT > 1 K, while the relationship is not evident for EΔBT < 1 K. This threshold is close to the value of 0.95 determined in Jia and Minnett [17] using the MUDB where data are mostly distributed at the Atlantic side of the Arctic. Note that there are some negative outliers at low EΔBT values, which were also found in Jia and Minnett [17], indicating the effects of

Preprints.org (www.preprints.org) | NOT PEER-REVIEWED | Posted: 6 May 2024 doi:10.20944/preprints202405.0250.v1

other error sources, such as undetected cloud contamination or improper atmospheric corrections. Most EΔBT values are < 1 K since water vapor effect in the BT difference can still be pronounced in summer. Due to the limited number of data, the relationship at large EΔBT, especially > 1.5 K, is not very solid. However, the patterns demonstrated here are encouraging since the theory of emissivity effect on MODIS SST_{skin} retrievals raised by Jia and Minnett [17] is further proven using SST_{skin} derivations from in situ measurements as validation data.

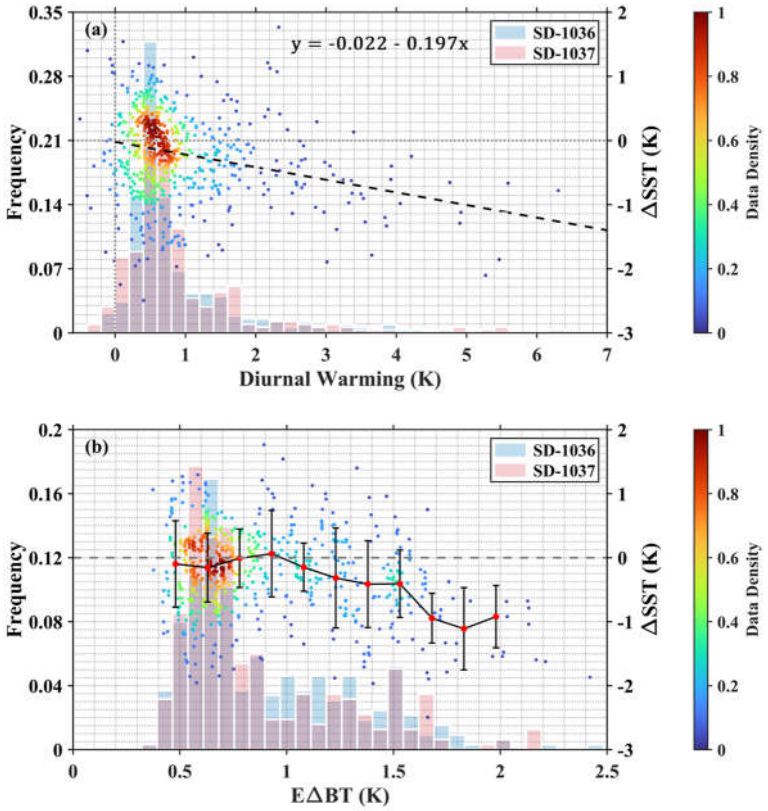

Figure 8. Scatter plots (colored by data density) of the Aqua MODIS-Saildrone SST_{skin} difference as a function of (a) the amplitude of diurnal warming with fitted black dashed line when diurnal warming exists and (b) the Emissivity-introduced BT difference (EΔBT) with red dots and error bars indicating the mean and STD of temperature differences, calculated at 0.16 K intervals. The histogram distributions of diurnal warming and EΔBT are also plotted as the background for the data during SD-1036 and SD-1037 cruises separately.

5. Conclusions

Accurate satellite-retrieved SST_{skin} is important for climate change studies and weather prediction, particularly for high latitude regions which draw attention due to the Arctic Amplification [50,51]. The deployment in the Pacific sector of the Arctic in the 2019 summer of two Saildrones carrying the "unicorn"-structured IR pyrometers on the deck, produced SST_{skin} with sufficient accuracy [29] which are used to validate the MODIS SST_{skin} retrievals in this study.

Multiple Saildrone measurements can be matched with the same MODIS pixel using the standard collocation time and space windows due to the high sampling frequency of Saildrone. Therefore, the Saildrone-MODIS matchup with the smallest separation is considered as the unique paired data for a high-quality MODIS pixel since the SST_{skin} biases are sensitive to the distance rather than time difference. The mean biases are significantly different (~0.4 K) for the matchups from the SD-1036 and SD-1037 data. Considering the relatively small numbers of comparisons and the divergent environmental conditions along the tracks of two Saildrones, the differences of large mean biases indicate statistics from neither of the two datasets are themselves representative of the characteristics of the conditions in the wider region of the Pacific Sector of the Arctic Ocean, and

 doi:10.20944/preprints202405.0250.v1

neither alone, would provide meaningful information about the capacities of the atmospheric correction algorithm when applied to MODIS measurements on a larger scale. But the combined data should provide a better representation. The statistics for MODIS on Aqua and Terra are very similar, even for the matchups with individual Saildrones, indicating that the performances of two MODIS sensors are comparable.

For further analysis of error characteristics, measurements with negative BT difference are discarded given the inappropriateness of the atmospheric correction algorithm. In addition, only data points measured above 60°N are analyzed to be consistent with the boundary of the high latitude band for algorithm coefficients. Overall, the average MODIS SST_{skin} biases for Aqua and Terra are -0.234 K and -0.295 K, with STDs of 0.677 K and 0.728 K. The negative biases in MODIS SST_{skin} retrievals are noteworthy. Due to the midnight sun in the Arctic summer, over 95% of total matchups are daytime data with possible presence of diurnal warming layers in the upper ocean. Figure 8a shows the MODIS SST_{skin} products are underestimated especially under large warming events > 2 K because of the lack of such conditions included in the derivation of the algorithm coefficients in Equation (1). Figure 8b demonstrates the MODIS SST_{skin} biases tend to be more negative when the surface emissivity effect is dominant in the BT difference between 11 μm and 12 μm bands, scaled by an index EΔBT, defined by Jia and Minnett [17]. The patterns in Figure 8b are similar to those found in Jia and Minnett [17], and it is very encouraging the retrieval errors resulting from the emissivity effect at high latitudes are further verified by the Saildrone-derived SST_{skin} data.

Additional research is necessary to improve the accuracy of IR SST_{skin} retrievals at high northern latitudes. Firstly, the causes of negative BT differences and their impact on the SST_{skin} retrieval should be investigated. A consequence of the current SST_{skin} retrievals in conditions where atmospheric temperature inversions occur leading to negative BT differences, is that spatial features in a satellite-derived SST_{skin} field are likely to contain contributions, probably significant and possibly dominant, from uncorrected atmospheric variability. It might be also possible the surface-generated aerosols contribute to the anomalous BT difference measurements, but here we lack aerosol data to examine such an effect, and so the possible influence of Arctic aerosols remains an open question, Moreover, the seemingly inappropriate cool skin correction using a constant value of -0.17 K for the MODIS SST_{skin} should be re-examined with more matchups with in situ SST_{skin} measurements, especially at night. The EΔBT index expression requires optimization, probably in terms of parameterizations of the relevant variables, refraining from running radiative transfer simulation for each pixel. Finally, more in situ SST_{skin} data with high accuracy at high latitudes are needed to further improve the understanding of inaccuracies in IR satellite-derived SST_{skin} and to refine the algorithms for satellite SST_{skin} retrievals in this challenging but vitally important area.

Author Contributions: Conceptualization, Chong Jia and Peter Minnett; Data curation, Chong Jia and Malgorzata Szczodrak; Formal analysis, Chong Jia; Funding acquisition, Peter Minnett; Methodology, Chong Jia and Peter Minnett; Project administration, Peter Minnett; Software, Chong Jia and Malgorzata Szczodrak; Supervision, Peter Minnett; Visualization, Chong Jia; Writing – original draft, Chong Jia; Writing – review & editing, Peter Minnett and Malgorzata Szczodrak.

Funding: This research was funded in part by a NASA contribution to the National Oceanographic Partnership Program (NOPP) Multi-sensor Improved Sea-Surface Temperature (MISST) project, Lead PI at the outset: Dr. Chelle Gentemann, The Farallon Institute, with Peter Minnett as a Co-I through contract 80NSSC20K0768, and by NASA grant 80NSSC21K1514 with Peter Minnett as PI. Chong Jia MS was a University of Miami Graduate School Fellow.

Data Availability Statement: MODIS on Aqua Level-2 SSTskin data files are available from: https://podaac.jpl.nasa.gov/dataset/MODIS_A-JPL-L2P-v2019.0. MODIS on Terra Level-2 SSTskin data files are available from: https://podaac.jpl.nasa.gov/dataset/MODIS_T-JPL-L2P-v2019.0. The Saildrone-derived SSTskin data are available at https://doi.org/10.17604/jnvv-nm74. The data for the 2019 Saildrone Arctic Cruises are available at https://doi.org/10.5067/SDRON-NOPP0. The reanalysis MERRA-2 data used in this study are available at https://doi.org/10.5067/WWQSXQ8IVFW8 and https://doi.org/10.5067/3Z173KIE2TPD.

Acknowledgments: We acknowledge the support of Saildrone Inc.

Conflicts of Interest: The authors declare no conflict of interest.

 doi:10.20944/preprints202405.0250.v1

References

1. Hardman-Mountford, N.J., et al., Ocean climate of the South East Atlantic observed from satellite data and wind models. Progress in Oceanography, 2003. 59(2): p. 181-221.
2. Merchant, C.J., et al., Satellite-based time-series of sea-surface temperature since 1981 for climate applications. Scientific Data, 2019. 6(1): p. 223.
3. Banzon, V., et al., A long-term record of blended satellite and in situ sea-surface temperature for climate monitoring, modeling and environmental studies. Earth Syst. Sci. Data, 2016. 8(1): p. 165-176.
4. Babin, S.M., et al., Satellite evidence of hurricane-induced phytoplankton blooms in an oceanic desert. Journal of Geophysical Research: Oceans, 2004. 109(C3).
5. Stramma, L., P. Cornillon, and J.F. Price, Satellite observations of sea surface cooling by hurricanes. Journal of Geophysical Research: Oceans, 1986. 91(C4): p. 5031-5035.
6. Lee, T. and M.J. McPhaden, Increasing intensity of El Niño in the central-equatorial Pacific. Geophysical Research Letters, 2010. 37(14).
7. Thomas, A.C., et al., Satellite-measured chlorophyll and temperature variability off northern Chile during the 1996–1998 La Niña and El Niño. Journal of Geophysical Research: Oceans, 2001. 106(C1): p. 899-915.
8. Casey, K.S., et al., The Past, Present, and Future of the AVHRR Pathfinder SST Program, in Oceanography from Space: Revisited, V. Barale, J.F.R. Gower, and L. Alberotanza, Editors. 2010, Springer Netherlands: Dordrecht. p. 273-287.
9. Kilpatrick, K.A., et al., A decade of sea surface temperature from MODIS. Remote Sensing of Environment, 2015. 165: p. 27-41.
10. Minnett, P.J., et al., Skin Sea-Surface Temperature from VIIRS on Suomi-NPP—NASA Continuity Retrievals. Remote Sensing, 2020. 12(20).
11. Coppo, P., et al., SLSTR: a high accuracy dual scan temperature radiometer for sea and land surface monitoring from space. Journal of Modern Optics, 2010. 57(18): p. 1815-1830.
12. Wang, H., L. Guan, and G. Chen, Evaluation of Sea Surface Temperature From FY-3C VIRR Data in the Arctic. IEEE Geoscience and Remote Sensing Letters, 2016. 13(2): p. 292-296.
13. Donlon, C., et al., Successes and challenges for the modern sea surface temperature observing system. Proceedings of OceanObs'09: Sustained Ocean Observations and Information for Society (Vol. 2), 2010.
14. O'Carroll, A.G., et al., Observational Needs of Sea Surface Temperature. Frontiers in Marine Science, 2019. 6: p. 420.
15. Shupe, M.D., et al., Clouds at Arctic Atmospheric Observatories. Part I: Occurrence and Macrophysical Properties. Journal of Applied Meteorology and Climatology, 2011. 50(3): p. 626-644.
16. Høyer, J.L., et al., Multi sensor validation and error characteristics of Arctic satellite sea surface temperature observations. Remote Sensing of Environment, 2012. 121: p. 335-346.
17. Jia, C. and P.J. Minnett, High latitude sea surface temperatures derived from MODIS infrared measurements. Remote Sensing of Environment, 2020. 251: p. 112094.
18. 18. Castro, S.L., G.A. Wick, and M. Steele, Validation of satellite sea surface temperature analyses in the Beaufort Sea using UpTempO buoys. Remote Sensing of Environment, 2016. 187: p. 458-475.
19. Vincent, R.F., The Case for a Single Channel Composite Arctic Sea Surface Temperature Algorithm. Remote Sensing, 2019. 11(20).
20. Donlon, C.J., et al., The global ocean data assimilation experiment high-resolution sea surface temperature pilot project. Bulletin of the American Meteorological Society, 2007. 88(8): p. 1197-1214.
21. Saunders, P.M., The Temperature at the Ocean-Air Interface. Journal of Atmospheric Sciences, 1967. 24(3): p. 269-273.
22. Flament, P., et al., Amplitude and Horizontal Structure of a Large Diurnal Sea Surface Warming Event during the Coastal Ocean Dynamics Experiment. Journal of Physical Oceanography, 1994. 24(1): p. 124-139.
23. Gentemann, C.L., et al., Multi-satellite measurements of large diurnal warming events. Geophysical Research Letters, 2008. 35(22).
24. Minnett, P.J., et al., The Marine-Atmospheric Emitted Radiance Interferometer: A High-Accuracy, Seagoing Infrared Spectroradiometer. Journal of Atmospheric and Oceanic Technology, 2001. 18(6): p. 994-1013.
25. Jessup, A.T. and R. Branch, Integrated Ocean Skin and Bulk Temperature Measurements Using the Calibrated Infrared In Situ Measurement System (CIRIMS) and Through-Hull Ports. Journal of Atmospheric and Oceanic Technology, 2008. 25(4): p. 579-597.

26. Donlon, C., et al., An Infrared Sea Surface Temperature Autonomous Radiometer (ISAR) for Deployment aboard Volunteer Observing Ships (VOS). Journal of Atmospheric and Oceanic Technology, 2008. 25(1): p. 93-113.
27. Gentemann, C.L., et al., MISST: The Multi-Sensor Improved Sea Surface Temperature Project. Oceanography, 2009. 22(2): p. 76-87.
28. Gentemann, C.L., et al., Arctic MISST: Multi-sensor Improved Sea Surface Temperature: Continuing the GHRSST Partnership and Improving Arctic data, in AGU Fall Meeting. 2018: Washington, D.C. p. A24K-11.
29. Jia, C., et al., High Latitude Sea Surface Skin Temperatures Derived From Saildrone Infrared Measurements. IEEE Transactions on Geoscience and Remote Sensing, 2023. 61: p. 1-14.
30. Koutantou, K., P. Brunner, and J. Vazquez-Cuervo Validation of NASA Sea Surface Temperature Satellite Products Using Saildrone Data. Remote Sensing, 2023. 15, DOI: 10.3390/rs15092277.
31. Vazquez-Cuervo, J., et al. Using Saildrones to Validate Satellite-Derived Sea Surface Salinity and Sea Surface Temperature along the California/Baja Coast. Remote Sensing, 2019. 11, DOI: 10.3390/rs11171964.
32. Kilpatrick, K.A., et al., Alternating Decision Trees for Cloud Masking in MODIS and VIIRS NASA Sea Surface Temperature Products. Journal of Atmospheric and Oceanic Technology, 2019. 36(3): p. 387-407.
33. Luo, B., et al., Improving satellite retrieved night-time infrared sea surface temperatures in aerosol contaminated regions. Remote Sensing of Environment, 2019. 223: p. 8-20.
34. Walton, C.C., et al., The development and operational application of nonlinear algorithms for the measurement of sea surface temperatures with the NOAA polar-orbiting environmental satellites. Journal of Geophysical Research: Oceans, 1998. 103(C12): p. 27999-28012.
35. Gelaro, R., et al., The Modern-Era Retrospective Analysis for Research and Applications, Version 2 (MERRA-2). Journal of Climate, 2017. 30(14): p. 5419-5454.
36. Jia, C. and P.J. Minnett, Ocean Warm Skin Signals Observed by Saildrone at High Latitudes. Geophysical Research Letters, 2023. 50(7): p. e2022GL102384.
37. Xu, F. and A. Ignatov, In situ SST Quality Monitor (iQuam). Journal of Atmospheric and Oceanic Technology, 2014. 31(1): p. 164-180.
38. Chin, T.M., J. Vazquez-Cuervo, and E.M. Armstrong, A multi-scale high-resolution analysis of global sea surface temperature. Remote Sensing of Environment, 2017. 200: p. 154-169.
39. Donlon, C.J., et al., Toward improved validation of satellite sea surface skin temperature measurements for climate research. Journal of Climate, 2002. 15(4): p. 353-369.
40. Minnett, P.J., M. Smith, and B. Ward, Measurements of the oceanic thermal skin effect. Deep Sea Research Part II: Topical Studies in Oceanography, 2011. 58(6): p. 861-868.
41. Zhang, H., et al., Nighttime Cool Skin Effect Observed from Infrared SST Autonomous Radiometer (ISAR) and Depth Temperatures. Journal of Atmospheric and Oceanic Technology, 2020. 37(1): p. 33-46.
42. Castro, S.L., et al., The impact of measurement uncertainty and spatial variability on the accuracy of skin and subsurface regression-based sea surface temperature algorithms. Remote Sensing of Environment, 2010. 114(11): p. 2666-2678.
43. Jia, C., P.J. Minnett, and B. Luo, Significant Diurnal Warming Events Observed by Saildrone at High Latitudes. Journal of Geophysical Research: Oceans, 2023. 128(1): p. e2022JC019368.
44. Stein, A.F., et al., NOAA's HYSPLIT Atmospheric Transport and Dispersion Modeling System. Bulletin of the American Meteorological Society, 2015. 96(12): p. 2059-2077.
45. Hocking, J., et al., A new gas absorption optical depth parameterisation for RTTOV version 13. Geosci. Model Dev., 2021. 14(5): p. 2899-2915.
46. Alappattu, D.P., et al., Warm layer and cool skin corrections for bulk water temperature measurements for air-sea interaction studies. Journal of Geophysical Research: Oceans, 2017. 122(8): p. 6470-6481.
47. Luo, B., et al., Regional and Seasonal Variability of the Oceanic Thermal Skin Effect. Journal of Geophysical Research: Oceans, 2022. 127(5): p. e2022JC018465.
48. Merchant, C.J., et al., Retrieval characteristics of non-linear sea surface temperature from the Advanced Very High Resolution Radiometer. Geophysical Research Letters, 2009. 36(17).
49. Zhang, H., et al., Comparison of SST Diurnal Variation Models Over the Tropical Warm Pool Region. Journal of Geophysical Research: Oceans, 2018. 123(5): p. 3467-3488.

 doi:10.20944/preprints202405.0250.v1

50. Rantanen, M., et al., The Arctic has warmed nearly four times faster than the globe since 1979. Communications Earth & Environment, 2022. 3(1): p. 168.
51. Serreze, M.C. and R.G. Barry, Processes and impacts of Arctic amplification: A research synthesis. Global and Planetary Change, 2011. 77(1): p. 85-96.